Hadronic mass spectrum in pseudofermion lattice QCD

M. Campostrini
Istituto Nazionale di Fisica Nucleare, Sezione di Pisa, Pisa 156100, Italy,
Dipartimento di Fisica, Università di Pisa, Pisa 156100, Italy,
and Department of Physics, Boston University, Boston, Massachusetts 02215

K. J. M. Moriarty
Institute for Advanced Study, Princeton, New Jersey 08540,
John von Neumann National Supercomputer Center, 665 College Road East, Princeton, New Jersey 08540,
and Department of Mathematics, Statistics, and Computing Science, Dalhousie University,
Halifax, Nova Scotia, Canada B3H 3J5

J. Potvin
Department of Physics, Boston University, Boston, Massachusetts 02215
and Department of Mathematics, Statistics, and Computing Science, Dalhousie University,
Halifax, Nova Scotia, Canada B3H 3J5

C. Rebbi
Department of Physics, Boston University, Boston, Massachusetts 02215
(Received 28 August 1989)

We report on a large-scale calculation of the hadronic mass spectrum in lattice quantum chromodynamics with dynamical quarks using the pseudofermion algorithm. The calculation was carried out on a $10^3\times 32$ lattice, at a gauge coupling of $\beta=5.70$, with three flavors of staggered quarks of mass $(ma)=0.05$ and 0.10 (in lattice units), and with four values of the acceptance: i.e., 60%, 70%, 81%, and 89%. The hadron masses were obtained from propagators calculated at mass $\bar{m}a=ma$, but also at $\bar{m}a=0.50$ and 0.02, in order to study hadronic states with different valence and dynamical quark masses. We also present the results of a calculation on a $10^3\times 24$ lattice at $\beta=5.47$ and $ma=0.05$ carried out for comparison with the results obtained by Gottlieb, Liu, Toussaint, Renken, and Sugar using the hybrid algorithm. Finally, we suggest a new parameter for a better estimate of the accuracy of the approximations involved in the pseudofermion algorithm.

I. INTRODUCTION

The numerical simulation of quantum chromodynamics (QCD) using lattice techniques offers the exciting possibility of deriving the low-energy properties of the strong interactions from first principles. Quantitative predictions can be made, and although these require the use of some approximations, the approximations themselves can be gradually relaxed in a controlled and systematic way.

Over the years, many simulations of lattice QCD have been devoted to the calculation of the hadronic mass spectrum (see the review papers of Refs. 1–3). Most have been performed in the valence, or quenched, approximation,[4] where the contributions from the creation and annihilation of light quark pairs have been neglected. Such an approximation can be justified on phenomenological and theoretical grounds [Okubo-Zweig-Iizuka (OZI) rule, large-N_c expansion]; it also allows substantial savings in computer time, which in turn permits the use of ever-increasing lattice volumes (now up to $V=18^3\times 42$) and gauge couplings (up to $\beta=6.2$), and decreasing quark masses (ma down to 0.02) (Refs. 5 and 6). The quenched approximation has also been used in comparisons between the staggered quarks and Wilson formulation of hadron propagators[6] and in the exploration of improved actions.[7] Ultimately, the comparison of the results from a calculation obtained in the valence approximation with those of QCD should yield a wealth of new information on the respective contributions of the gluons and quarks.

Lattice QCD calculations have so far confirmed the Goldstone nature of the pion, and also reproduced qualitatively the salient features of the hadronic mass spectrum (absence of pionic states of opposite parity, restoration of flavor symmetry in the staggered formulation, etc.).[1–3] At a more quantitative level, however, the mass ratios of proton to ρ and of pion to ρ are systematically higher than the experimental values by 30% and more. In most of these calculations, the quark masses are of order 50–150 MeV and typical lattice spacings are of order 0.10 fm.

Although very demanding in computer resources, there have been several attempts at simulating QCD in the presence of dynamical quarks.[8–14] Most have been done using two, three, and four flavors of dynamical staggered quarks, on volumes ranging from $8^3\times 16$ to $10^3\times 32$. Limitations in computer time have restricted

the values of possible quark masses to the range $0.025 \leq ma \leq 0.10$, and those of the gauge coupling to $5.20 \leq \beta \leq 5.6$. Finally, most calculations were done using one of the three algorithms that implement the contribution of the $q\bar{q}$ pair creation and/or annihilation in a fast but approximate way, i.e., the pseudofermion, Langevin and hybrid algorithms.

The hadronic mass spectrum obtained from these studies has been found to be consistent, within 10% error, with that of the quenched approximation. At this level of accuracy and for the values of the quark masses and gauge couplings being considered, it appears that the effect of the dynamical fermions mostly amounts to a renormalization of the coupling in a quenched simulation.[8,9]

These conclusions, of course, must change drastically as the continuum limit is approached since, with the use of larger couplings and smaller quark masses, the pion will reach a mass low enough to permit the decay $\rho \rightarrow 2\pi$. Moreover, one anticipates that the systematic errors due to the shrinking of the lattice spacing and to the updating algorithm will be much more severe than what has been seen so far. It will therefore be very important, as we proceed towards the continuum limit, to continue monitoring the effects of these systematic errors on the spectrum.

It is in this spirit that we present the results of our own calculation of low-energy hadronic spectroscopy, done on a $10^3 \times 32$ lattice. We have used three flavors of staggered dynamical quarks of mass $ma = 0.05$ and 0.10, at a value of the coupling larger than what has been used before, i.e., $\beta = 5.70$. The contributions of the $q\bar{q}$ pair creation and/or annihilation have been included in the calculation through the use of the pseudofermion algorithm, which we have run at four values of the acceptance (60%, 70%, 81%, and 89%) in order to study the effects of the systematic errors. Finite-size effects were monitored by a calculation of the spatial Polyakov line at each value of the quark mass and the acceptance. The hadronic propagators were calculated in the background gauge field, using a source mass of $\bar{m}a = 0.50$, 0.10, 0.05, and 0.02. Finally, in order to further address the accuracy of the pseudofermion algorithm on the hadronic mass spectrum, we have carried out another calculation at $\beta = 5.47$, $ma = 0.05$ (two flavors), acceptance 81% and 90%, on a $10^3 \times 24$ lattice for comparison with the results of a calculation by Gottlieb, Liu, Toussaint, Renken, and Sugar[13] done with the hybrid algorithm at the same values of β, mass and lattice size.

Some of the results presented here have been reported and briefly discussed elsewhere.[15,16] These, as well as new data obtained at other values of the gauge coupling, quark masses, acceptance and lattice volumes, will be discussed in more detail in this paper, which is organized as follows. In Sec. II we describe briefly the various methods used in the update of the gauge fields and in the analysis of the hadron propagators. In Sec. III we discuss the various systematic errors encountered in our calculation and how we have managed to control them. In Sec. IV we report on our main results: i.e., the hadron mass spectrum, the inverse lattice spacing associated with our choice of gauge couplings, the mass ratios of proton to ρ and of π to ρ, and several masses of heavy (or "charmed") hadrons. Finally, we present our conclusions in Sec. V.

II. ALGORITHMS

A. The pseudofermion algorithm

So far, most mass spectroscopy calculations in lattice QCD with dynamical fermions have been done with approximate but fast algorithms, which can be divided into two groups: those based on the Metropolis approach, such as the pseudofermion[17] and the bush factorized[18] algorithms, and those based on the iteration of a stochastic or deterministic equation of motion, such as the Langevin and the hybrid[19] methods. All these algorithms introduce some systematic errors which must be kept under control.[2] (A calculation using the exact hybrid Monte Carlo algorithm[20] has been reported in Ref. 12.)

The formulation of QCD on the lattice is defined by the following path integral, here written with the fermionic degrees of freedom integrated out:

$$Z = \int [dU] \det(M^\dagger[U] M[U])^{n_f/8} \exp(-S_G[U]) \tag{2.1}$$

$$= \int [dU] \exp\left[-S_G + \frac{n_f}{8} \mathrm{Tr} \ln(M^\dagger M) \right] . \tag{2.2}$$

The gauge fields are represented by the link variables $U \equiv U_x^\mu$, and $M[U] \equiv (D[U] + ma)$ is the lattice Dirac operator in the staggered quark formulation. The integer n_f is the number of flavors and S_G stands for Wilson's pure gauge action. For more details on our notation and conventions, see Refs. 16 and 17.

In the quenched approximation, the evaluation of Eq. (2.1) is drastically simplified by assuming $\det(M^\dagger M) = 1$. In recent years practical schemes have been introduced to calculate the contribution from this determinant to Eq. (2.1). The pseudofermion method of Fucito, Marinari, Parisi, and Rebbi[17] is one such algorithm. Since it has been discussed extensively in the literature[18,21–23] we review here only its salient features.

The pseudofermion algorithm is a Metropolis procedure[24] in which the link variables U_x^μ are tentatively changed into $U_x'^\mu$, which we have chosen to define as

$$U_x'^\mu = R_x^\mu U_x^\mu, \quad R_x^\mu = \exp(i\rho\theta^i\lambda_i) . \tag{2.3}$$

The θ^i's are normal Gaussian random numbers, the λ_i's are Gell-Mann matrices, and ρ is a real number representing the step size. This proposed change is accepted or rejected depending on the size of the variation of the full effective action S:

$$\delta S = S[U'] - S[U]$$

$$= \delta S_G + \frac{n_f}{8} \mathrm{Tr}[\ln(M^{\dagger\prime} M') - \ln(M^\dagger M)] . \tag{2.4}$$

In the pseudofermion algorithm, δS is approximated by a first-order approximation to the logarithm in Eq. (2.4):

$$\delta S \simeq \delta S_G + \frac{n_f}{8}\mathrm{Tr}\{[D(\delta D^\dagger)+(\delta D)D^\dagger]/[(ma)^2+DD^\dagger]\} . \tag{2.5}$$

Here $\delta D \equiv D[U']-D[U]$. A second approximation involves the use of the same matrix $[(ma)^2+DD^\dagger]^{-1}$ to update all the links in a given sweep through the lattice. Finally the inverse of the matrix $[(ma)^2+DD^\dagger]$ is calculated via an "internal" Monte Carlo simulation of a path integral featuring the bosonic variables $\phi(x)$ (the so-called pseudofermions) and an action $\bar{\phi}[(ma)^2+DD^\dagger]\phi$:

$$(MM^\dagger)^{-1}_{ij} = \frac{1}{Z_\phi}\int [d\bar{\phi}][d\phi]\bar{\phi}_i\phi_j e^{-\bar{\phi}[(ma)^2+DD^\dagger]\phi} . \tag{2.6}$$

The errors due to the approximation introduced in Eq.(2.5) and the use of $[(ma)^2+DD^\dagger]^{-1}$ for all updates in a sweep are eliminated, as shown in Sec. III, in the limit of zero step size $\delta \to 0$, for which the acceptance, or the ratio of accepted over proposed changes, is 100%. The elimination of the errors introduced by the internal Monte Carlo simulation [Eq. (2.6)] requires in principle that the number of pseudofermionic sweeps N_{pf} becomes very large, but it can be argued that their effects also decrease, for fixed N_{pf}, as the acceptance increases. (This requires, of course, that every sequence of pseudofermionic upgradings begins with the final values from the previous sequence, but any sensible code would implement that.)

Our calculation was performed using several values of ρ, i.e., 0.105, 0.075, 0.048, and 0.023, which corresponded to 60%, 70%, 81%, and 89% acceptance, respectively. See Tables I(a)–I(c) for more details on the values of the parameters used in our calculation and Ref. 16 for the details of our implementation of the algorithm. In a given sweep, each link was updated with eight Metropolis hits. The inner Monte Carlo simulation was implemented by a parallel heat-bath upgrading of all the pseudofermions defined on random sets of statistically independent sites. This procedure was chosen so as to achieve long vector lengths (on a Cyber 205) and to avoid possible biases due to a systematic scanning of the pseudofermionic variables.[16] Here the selected average number of pseudofermion sweeps was effectively equal to $N_{\mathrm{pf}}=24$.

The pseudofermion algorithm has been tested for various simple models,[23] and for several values of the quark mass on small lattices.[21,22] These studies have shown that the algorithm can be inaccurate for small values of the quark masses (i.e., $ma \leq 0.10$) even at standard values of the acceptance (60% to 85%). On the other hand, the errors of the internal Monte Carlo simulation appeared to be under control for $N_{\mathrm{pf}} \geq 20$. It is therefore important to be able to devise a way to monitor the magnitude of the errors due to the acceptance or, alternatively, to be able to extract the exact operator averages from the results obtained at $\rho \neq 0$. This will be shown in more detail in Sec. III.

B. Hadron masses

The hadron masses are obtained from the quark propagators M^{-1} according to a procedure which is now well established.[25] It consists in forming first meson and baryon propagators, which in the staggered quarks formulation have the form

TABLE I. Simulation parameters.

$\rho/(ma)^2$	Acc (%)	No. iterations	Hadron propagators (measurement interval)
	(a) $\beta=5.70$, $V=10^3\times 32$, $n_f=3$, $ma=0.10$		
7.50	70	18 500	Yes(500)
4.80	81	17 500	Yes(500)
2.00	92	11 000	No
	(b) $\beta=5.70$, $V=10^3\times 32$, $n_f=3$, $ma=0.05$		
52.0	50	9 000	No
42.0	60	8 000	No
30.0	70	15 000	Yes(500)
19.2	81	19 000	Yes(500)
10.8	89	41 000	Yes(1000)
	(c) $\beta=5.47$, $V=10^3\times 24$, $n_f=2$, $ma=0.05$		
19.2	81 (ordered start)	6 250	No
19.2	81 (random start)	10 450	Yes(500)
8.00	92	13 000	No

$$P^{m(k)}_{x_0}=\sum_{c,c_0} S_{(k,x)}M^{-1}_{xc,x_0c_0}M^{-1*}_{xc,x_0c_0} \tag{2.7}$$

and

$$P^{b(k)}_{xx_0}=\sum_{c_1,c_2,c_3} S_{(k,x)}\epsilon_{c_1,c_2,c_3}M^{-1}_{xc_1,x_01}M^{-1}_{xc_2,x_02}M^{-1}_{xc_3,x_03}\ . \tag{2.8}$$

The index c_i corresponds to SU(3) color; the $S_{(k,x)}$ are suitable spin factors. The latter are defined as

$$\begin{aligned} S_{(1,x)}&=1\ ,\\ S_{(2,x)}&=(-1)^{n_x}+(-1)^{n_y}+(-1)^{n_z}\ ,\\ S_{(3,x)}&=(-1)^{n_x+n_y}+(-1)^{n_z+n_x}+(-1)^{n_y+n_z}\ ,\\ S_{(4,x)}&=(-1)^{n_x+n_y+n_z}\ , \end{aligned} \tag{2.9}$$

and act as (unnormalized) projection operators over states of definite hadronic quantum numbers. In particular, $P^{m(1)}$ overlaps with states of $J^{PC}=0^{+-}$ pion quantum numbers, $P^{m(2)}$ with mesonic states of the $\rho(1^{--})$ and $b_1(1^{+-})$, $P^{m(3)}$ with mesonic states of the $\rho(1^{--})$ and $a_1(1^{++})$ and finally $P^{m(4)}$ with states of the $\pi(0^{+-})$ and the $f_0(0^{++})$ mesons. On the other hand, the operator $P^{b(k)}$ will produce overlaps with states of nucleon and $\frac{1}{2}^-$ baryon quantum numbers.

The hadron masses are calculated by averaging first the $P^{b(k)}$'s and $P^{m(k)}$'s over the spatial coordinate $\mathbf{x}$, thereby resulting in zero-momentum propagators $G^{b,m(k)}_{tt_0}$, and then extracting the exponential decay of the latter through a fit with the form ($N_t=32$)

$$G^{m(k)}_{t,t_0=0}=\sum_n A_n(e^{-m_n t}+e^{-m_n(32-t)}) +(-1)^t\sum_n \tilde{A}_n(e^{-\tilde{m}_n t}+e^{-\tilde{m}_n(32-t)})\ , \tag{2.10}$$

$$G^{p(k)}_{t,t_0}=\sum_n \{\ A_n[e^{-m_n t}+(-1)^t e^{-m_n(32-t)}] +\tilde{A}_n[(-1)^t e^{-m_n t}+e^{-m_n(32-t)}]\}\ . \tag{2.11}$$

The terms in A_n and $\tilde{A}_n$ represent the states in the direct and opposite parity channels, respectively, a peculiarity of the staggered quarks formulation. The exponential with argument $[-m_n(32a-t)]$ corresponds to the fact that periodic boundary conditions have been used in our calculation. Fitting the average $\langle G\rangle$ out of $N_{\rm tot}$ propagators to form Eq. (2.10) with a program which minimizes the χ^2 thus produces the hadron masses $m_n,\tilde{m}_n$ and amplitudes $A_n,\tilde{A}_n$ as output variables. The errors on the masses were obtained from a jackknife analysis,[26]

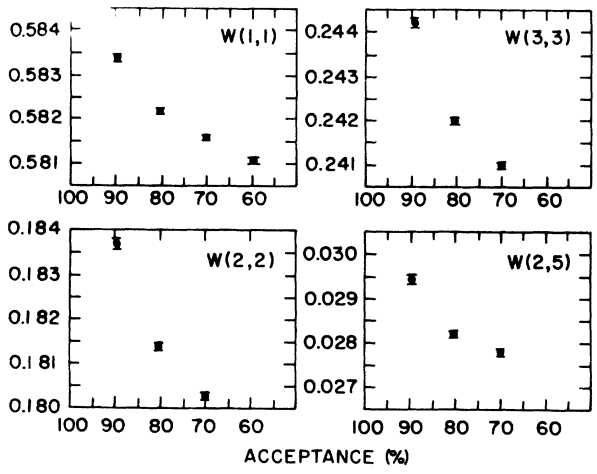

FIG. 1. Wilson loop factors vs the acceptance with $ma=0.05$, $n_f=3$, $\beta=5.70$, and $V=10^3\times 32$.

in which more hadron masses are extracted from χ^2 fits of sets of propagators containing all but $\bar{N}$ consecutive propagators in the measurement sequence, out of a total of N propagators. From the resulting set of $N/\bar{N}$ masses one computes the average $\langle(m_{\bar{N}}-\hat{m})^2\rangle$, where $\hat{m}$ is the average mass extracted from the analysis of all N propagators; the so-called "jackknife" error is then given by

$$(\Delta m)^2=\left[\frac{N}{N-\bar{N}}-1\right]\langle(m_{\bar{N}}-\hat{m})^2\rangle\ .$$

III. SYSTEMATIC ERRORS

In Sec. II we have enumerated the different sources of systematic errors which may affect the updating of the gauge configurations, as well as the results of the fits to the hadron propagators. In this section we take a closer look at these issues and show how they have been eliminated or controlled in our calculation.

A. First-order discretization and the pseudofermion algorithm

As shown in Fig. 1 and in many other studies,[21–23] various physical quantities such as the Wilson loop exhibit some dependence on ρ (or equivalently on the acceptance). Such a variation similarly occurs in the Langevin and hybrid algorithms, relative to the discretization step size $\Delta\tau$ (Refs. 8 and 19).

In a Metropolis updating step, the probability of accepting or rejecting the proposed change U' will be proportional to $\exp(-S[U']+S[U])$. In the fermion sector, this expression will have the form

$$\Delta_{\rm exact}=\exp\left\{\frac{n_f}{8}\mathrm{Tr}\ln\left[\left[1+\frac{D'D'^{\dagger}}{(ma)^2}\right]\Big/\left[1+\frac{DD^{\dagger}}{(ma)^2}\right]\right]\right\}, \tag{3.1}$$

$$\Delta_{\rm exact}=\exp\left[\frac{n_f}{8}\mathrm{Tr}\ln\left[1+\frac{D'D'^{\dagger}-DD^{\dagger}}{(ma)^2+DD^{\dagger}}\right]\right]. \tag{3.2}$$

Notice that

$$(D'D'^{\dagger}-DD^{\dagger})=[D(\delta D^{\dagger})+(\delta D)D^{\dagger}+(\delta D)(\delta D^{\dagger})]\propto\rho+\theta(\rho^2)\ . \tag{3.3}$$

If $D'D'^{\dagger}-DD^{\dagger}$ is smaller than the smallest eigenvalue of the operator $(ma)^2+DD^{\dagger}$, or approximately, if $\rho\ll(ma)^2$ and $\rho<1$, the logarithm can be Taylor expanded as

$$\Delta_{\text{exact}}=\exp\left\{\frac{n_f}{8}\mathrm{Tr}\left[(-1)\sum_{n=1}^{\infty}\frac{(-1)^n}{n}\left[\frac{D'D'^{\dagger}-DD^{\dagger}}{(ma)^2+DD^{\dagger}}\right]\right]^n\right\}, \tag{3.4}$$

and upon further expanding the exponential and using Eq. (3.3),

$$\Delta_{\text{exact}}=1+\frac{n_f}{8}\mathrm{Tr}\left[\frac{D(\delta D^{\dagger})+(\delta D)D^{\dagger}}{(ma)^2+DD^{\dagger}}\right]+\frac{n_f}{8}\mathrm{Tr}\left[\frac{\delta D\delta D^{\dagger}}{(ma)^2+DD^{\dagger}}\right]+\cdots+O_1\ . \tag{3.5}$$

O_1 denotes all the terms in higher order, i.e., $[\rho/(ma)^2]^{n\geq 2}$, $\rho[\rho/(ma)^2]^{n\geq 2}$, and $\rho^2[\rho/(ma)^2]^{n\geq 2}$. With a similar expansion using Eq. (2.5), the pseudofermion approximation Δ_{pf} will read

$$\Delta_{\text{pf}}=1+\frac{n_f}{8}\mathrm{Tr}\left[\frac{D(\delta D^{\dagger})+(\delta D)D^{\dagger}}{(ma)^2+DD^{\dagger}}\right]+\cdots+O\left[\rho\frac{\rho}{(ma)^2}\right]+O_1 \tag{3.6}$$

or

$$\Delta_{\text{pf}}=\Delta_{\text{exact}}-\frac{n_f}{8}\mathrm{Tr}\left[\frac{(\delta D)(\delta D^{\dagger})}{(ma)^2+DD^{\dagger}}\right]+\cdots+O_1\ . \tag{3.7}$$

Δ_{pf} and Δ_{exact} thus differ by terms of order $\rho[\rho/(ma)^2]$ and of order

$$\left[\frac{\rho}{(ma)^2}\right]^2,\ \rho\left[\frac{\rho}{(ma)^2}\right]^2,\ \rho^2\left[\frac{\rho}{(ma)^2}\right]^2\ \text{(and higher powers)}\ .$$

As mentioned earlier, using the same matrix $[(ma)^2+DD^{\dagger}]^{-1}$ for all the updates in the same Metropolis sweep will introduce an additional relative error. Considering the second term on the right-hand side of Eqs. (3.5) and (3.6), for example, one has the extra term

$$[D(\delta D^{\dagger})+(\delta D)D^{\dagger}]\delta\left[\frac{1}{(ma)^2+DD^{\dagger}}\right]\sim[D(\delta D^{\dagger})+(\delta D)D^{\dagger}]^2\left[\frac{1}{(ma)^2+DD^{\dagger}}\right]^2\sim\frac{\rho^2}{(ma)^4}\ . \tag{3.8}$$

Including this source of error in $\Delta_{\text{pf}}-\Delta_{\text{exact}}$ will generate more terms, proportional to an extra factor $\rho/(ma)^2$ with respect to those enumerated in Eq. (3.7).

What comes out clearly from this discussion is the fact that the probability of acceptance in the pseudofermion algorithm does not depend on ρ alone, but on the ratio $\rho/(ma)^2$ at the lowest order. Consequently, it makes more sense to extrapolate the results of a pseudofermion simulation with respect to $\rho/(ma)^2$. This is particularly important in QCD, where the quark masses ma, along with ρ, are also tuned to smaller values. An extrapolation to $ma\to 0$ at fixed ρ will involve large variations in the difference $|\Delta_{\text{pf}}-\Delta_{\text{exact}}|$, thereby losing any control on the systematic error. The correct approach should involve an extrapolation to $\rho=0$ first, and then $ma=0$.

Figure 2 shows how our data at $\beta=5.70$ change with $\rho/(ma)^2$. Figure 2 [see also Table II(a)] shows that the ρ dependence of the Wilson loop of $W(1,1)$ is strongly mass

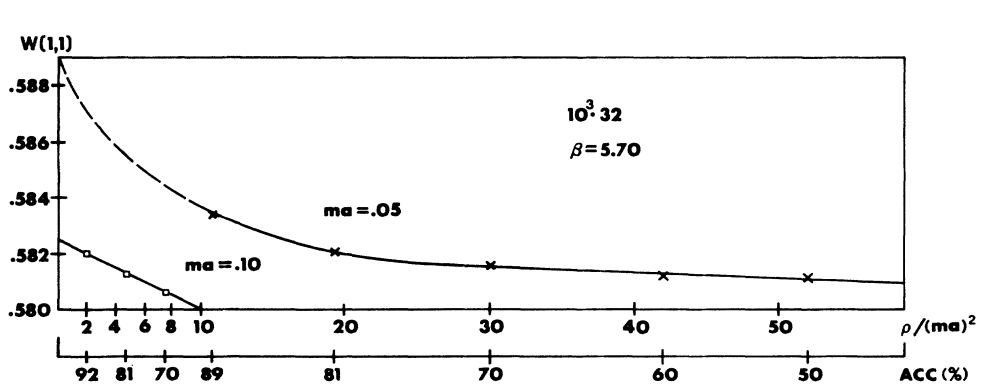

FIG. 2. Wilson loop factors vs $\rho/(ma)^2$ and the quark mass. The lower abcissa shows the corresponding acceptances for $ma=0.10$ (acc: 92 to 70 on the left) and for $ma=0.05$ (acc: 89 to 50, on the right). The continuous and dashed lines are to guide the eye.

dependent. It appears that a linear extrapolation may be possible in the case of $ma=0.10$. However, it has to be pointed out that the values of the ratio $\rho/(ma)^2$ are all greater than 1 and thus outside the validity range of the $\rho/(ma)^2 \ll 1$ limit discussed above. A linear extrapolation from these data can only be validated if points for which $\rho/(ma)^2 < 1$ can be included.

Figure 2 shows that, clearly, a linear extrapolation is out of the question for our data at $ma=0.05$, regardless of the fact that supposedly "high" acceptances of 70% up to 90% have been used in the simulation. Here the dashed and continuous lines are to guide the eye. Figure 2 also suggests that looking for small variations of the Wilson loop in order to choose a single optimal value of the acceptance to run a simulation, as done in the past, may also be hazardous.

Although the plaquette data do not prove as yet the usefulness of the ratio $\rho/(ma)^2$ as a parametrization of the updating systematic error, we feel that it is far more objective than monitoring the acceptance only, in that it can be related directly to the two major sources of error, i.e., the step size ρ and lowest eigenvalue of the operator $(m^2+DD^\dagger)$.

The dependence of the hadronic mass spectrum on $\rho/(ma)^2$ may be substantial as well, as shown in Fig. 3. The data at $ma=0.10$ show a clear variation towards smaller ρ. Depending on the state, a variation of 2–10% seems to take place between the finite-ρ values and the limiting values for $\rho=0$, as suggested by a linear extrapolation where one obtains 0.74(3), 0.77(5), 0.87(4), 0.82(5), 1.03(4), 1.20(4), and 1.31(3) for the $\pi,\pi',\rho,\rho',f_0,a_1$ and baryon, respectively. The errors associated with the $ma=0.05$ data are too large to yield a meaningful extrapolation. What can be done, however, is to get a rough

TABLE II. Wilson loop factors vs the acceptance.

(a)

$\beta=5.70$, $V=10^3\times 32$, $n_f=3$, $ma=0.10$

$W(R,T)$	Acc (%): 70	81	92
1×1	0.580 766(37)	0.581 365(47)	0.582 103(105)
1×2	0.369 269(55)	0.370 190(72)	0.371 300(150)
1×3	0.239 727(60)	0.240 740(75)	0.241 917(173)
2×2	0.178 821(74)	0.179 923(89)	0.181 090(179)
2×3	0.093 618(71)	0.094 598(81)	0.095 532(171)
3×3	0.042 559(62)	0.043 336(68)	0.043 979(135)
3×4	0.020 320(49)	0.020 787(53)	0.021 241(112)
4×4	0.008 825(36)	0.009 168(39)	0.009 374(81)
5×5	0.001 651(21)	0.001 737(25)	0.001 819(39)

(b)

$\beta=5.70$, $V=10^3\times 32$, $n_f=3$, $ma=0.05$

$W(R,T)$	Acc (%): 50	60	70	81	89
1×1	0.581 226(48)	0.581 361(77)	0.581 594(45)	0.582 183(45)	0.583 549(62)
1×2	0.369 755(64)	0.369 962(115)	0.370 461(64)	0.371 455(68)	0.373 546(97)
1×3	0.240 146(73)	0.240 447(123)	0.241 023(70)	0.242 074(73)	0.244 381(110)
2×2	0.179 346(83)	0.179 697(140)	0.180 323(77)	0.181 417(88)	0.184 003(124)
2×3	0.094 013(79)	0.094 432(145)	0.094 926(65)	0.095 844(75)	0.098 187(110)
3×3	0.042 892(70)	0.043 244(132)	0.043 505(58)	0.044 275(67)	0.046 189(81)
3×4	0.020 501(48)	0.020 830(121)	0.021 038(49)	0.021 431(53)	0.022 763(68)
4×4	0.008 967(42)	0.009 152(91)	0.009 344(34)	0.009 485(42)	0.010 440(43)
5×5	0.001 697(35)	0.001 757(40)	0.001 819(33)	0.001 845(32)	0.002 200(45)

(c)

$\beta=5.47$, $V=10^3\times 24$, $n_f=2$, $ma=0.05$

$W(R,T)$	Acc (%): 81	92
1×1	0.534 567(178)	0.538 114(202)
1×2	0.308 720(236)	0.313 499(293)
1×3	0.181 466(227)	0.186 006(295)
2×2	0.120 480(232)	0.125 225(282)
2×3	0.050 458(175)	0.053 722(216)
3×3	0.016 197(113)	0.018 025(127)
3×4	0.005 403(67)	0.006 232(71)
4×4	0.001 471(45)	0.001 819(51)
4×5	0.000 127(34)	0.000 081(35)

estimate by using the $ma=0.10$ pion mass at $\rho \to 0.0$, assume the relation $(m_\pi a)^2 \propto ma$ and interpolate at $ma=0.05$. We obtain then $m_\pi a=0.52(2)$, i.e., a 10% variation over the value at acceptance 80% and 90%.

B. Confinement versus deconfinement

The introduction of dynamical fermions will, in contrast to a quenched simulation, lower the average value of the action. Effectively, the fermions contribute in reducing the lattice spacing, thus inducing size effects similar to those involved in a simulation at nonzero temperature.

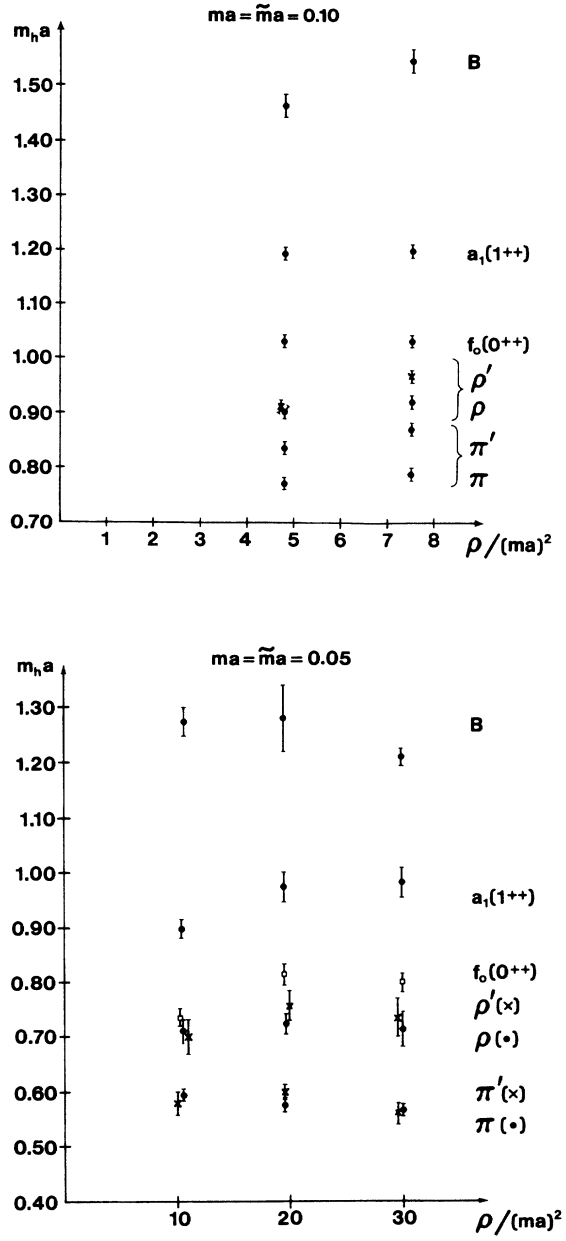

FIG. 3. Hadronic masses vs $\rho/(ma)^2$, for $ma=\tilde{m}a=0.10$ (top) and $ma=\tilde{m}a=0.05$ (bottom); $n_f=3$, $\beta=5.70$, and $V=10^3\times 32$.

It is therefore important to verify that the system is effectively on the confinement side, rather than on the deconfinement side, of the QCD high-temperature phase transition.

That dynamical quarks may induce a deconfinement transition on a small lattice has been demonstrated by Fukugita, Oyanagi, and Ukawa.[8] Using the Langevin algorithm at $\Delta\tau=0.01$ with $\beta=5.6, n_f=3$, $ma=0.05$ (and also 0.10), they have shown that the system does indeed go from the confinement phase to the deconfinement phase as the lattice size is decreased from $10^3\times 20$ to $8^3\times 18$. This transition was monitored via the Polyakov line L in each of the spatial directions, which shows clustering around the origin in the confinement phase and around one of the Z_3 axes in the deconfinement phase.

We have looked for finite-temperature effects in our calculation in two ways: first by comparing the Wilson loop from a simulation started with an ordered configuration with the Wilson loop from another simulation started with a random configuration (with acceptance 80%); both simulations gave the same value for the loop factors within errors, i.e., 0.582 192(43) and 0.582 104(65), respectively, thus supporting the absence of metastable states.

In our second approach, the Polyakov lines $\langle L \rangle$ have been calculated for all the measurement runs, in the three directions, at all values of the acceptance. Figures 4 and 5 show plots of $\mathrm{Im}\langle L \rangle$ vs $\mathrm{Re}\langle L \rangle$ for each of these cases. By and large, all show a strong clustering around the origin. Two plots at acceptance 90% and $ma=0.05$ and 0.10 show some degree of elongation, but by no means a clear clustering along any of the Z_3 axes. Overall, the plots of Figs. 4 and 5 have much the same characteristics (including the elongated plots of 90% acceptance) as those of Fukugita, Oyanagi, and Ukawa[8] at volume $10^3\times 20$. We therefore conclude that our data do not show any signal of finite-temperature effects.

Let us mention that approximate algorithms such as the Langevin or pseudofermion methods could fail to show deconfinement even when this could be legitimately expected. Because these algorithms tend to produce more disordered gauge configurations, a too large value of $\Delta\tau$ or ρ could effectively lower the temperature. But because we do not see any clear evolution of our Polyakov lines toward a deconfinement state as the acceptance is increased, we conclude that the spatial volume of 10^3 should be large enough to support confinement at $\beta=5.70$ with $n_f=3$ and $ma=0.05, 0.10$.

C. Autocorrelations

Turning to smaller values of ρ increases the accuracy of the pseudofermion algorithm. But then the evolution in the SU(3) space of link variables becomes slower and thus the autocorrelations between successive Monte Carlo configurations increase.

We have looked for autocorrelations in the Wilson loops, which were calculated every ten Metropolis sweeps (see Table II). The samples of 1200, 1700, 3900 loops, for acceptance 70%, 81%, 89%, respectively, were grouped and averaged in bins of several sizes and the variance

over the averages calculated. By locating the onset of a plateau in the variance with respect to bin size one gets a good estimate of the autocorrelation length in the Wilson loop data. Figure 6 shows such onsets for various loop sizes at acceptance 80% ($ma=0.05$ here). The autocorrelation lengths at 89% acceptance (300 to 500 sweeps) seem to be 3 to 4 times those at 70% and 81% (100 to 200 sweeps). This information has been used in our calculation of the error by the jackknife method,[26] in setting the proper number of points to be removed.

We have also studied the autocorrelations between the measurements of the pion propagator. Figure 7 shows this quantity on time slice 17 versus the Metropolis sweeps. The propagators were calculated every 500 (70%, 81% acceptance) and 1000 (89%) iterations. The results show the presence of autocorrelation intervals of order 2000 to 4000 iterations, depending on the acceptance. These intervals are of the same magnitude as those of the pseudofermion study of Born *et al.*[14] performed at $\beta=5.20, 5.35$, $n_f=4$ and $ma=0.025$, 85–92 %

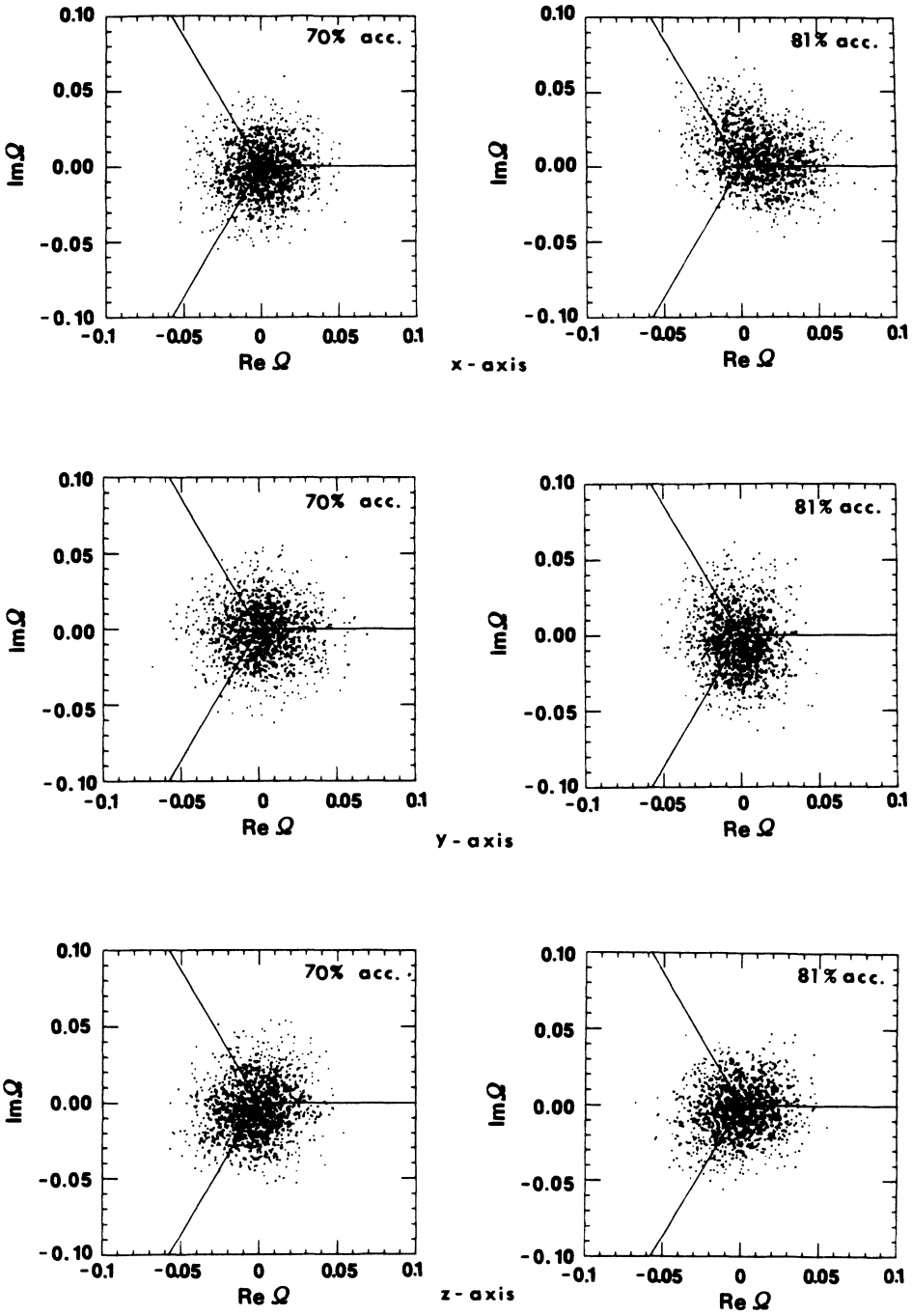

FIG. 4. Polyakov line in the complex plane. Here $ma=0.05$, $n_f=3$, $\beta=5.70$, and $V=10^3\times 32$.

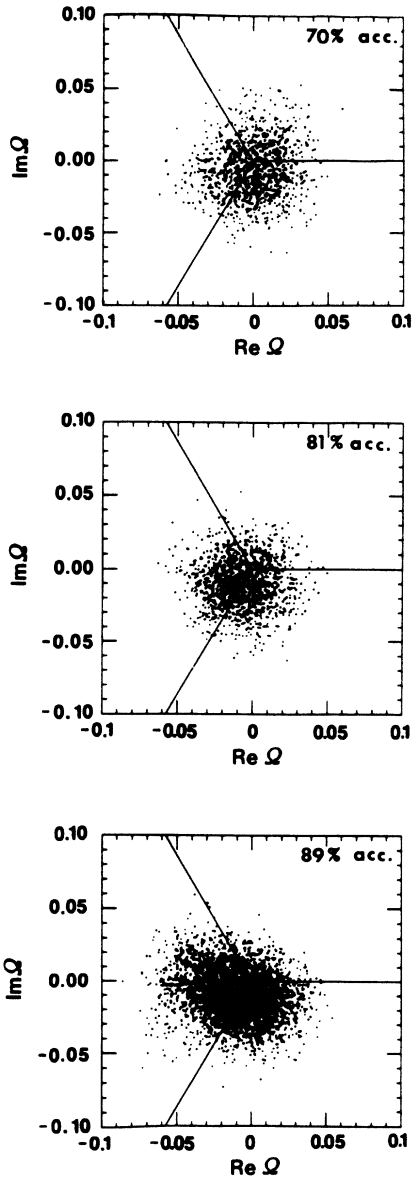

FIG. 5. Polyakov line in the complex plane. Here $ma=0.10$, $n_f=3$, $\beta=5.70$, and $V=10^3\times 32$.

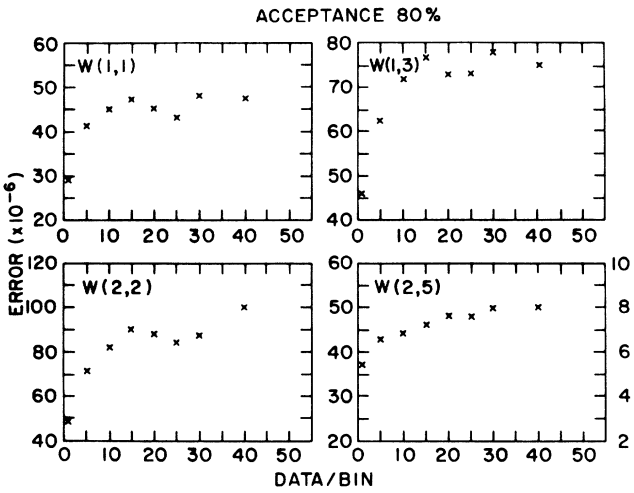

FIG. 6. Error on the Wilson loop factors, as a function of the number of data per analysis bin. Here $ma=0.05$, $n_f=3$, $\beta=5.70$, and $V=10^3\times 32$.

acceptance and one Metropolis hit per link. Effectively, their Metropolis random walk updating distance in SU(3) space is smaller than ours by a factor 2 (we use eight Metropolis hits per link), but their evolution could be faster since Born *et al.* have used a large gauge coupling g ($\beta=6/g^2$).

A similar comparison of the autocorrelation intervals in the pion propagator can be done also with the Langevin data of Fukugita, Oyanagi, and Ukawa[8] ($10^3\times 24$, $n_f=2$, $ma=0.05$, $\beta=5.5$, $\Delta\tau=0.01$), where shorter intervals of about 500 iterations have been seen.

D. Mass spectrum analysis

Using the conjugate gradient algorithm,[27] we have calculated the inverse $(D+\tilde{m}a)^{-1}_{x_0x}$ every 500 or 1000 iterations, depending on the acceptance (Table I). That inverse was obtained for three different sources x_0, located at $x=1$, $y=1$, $z=1$, and $t=1$, 12, and 23 on the same gauge configuration. In the jackknife analysis, only the three propagators corresponding to these three sources

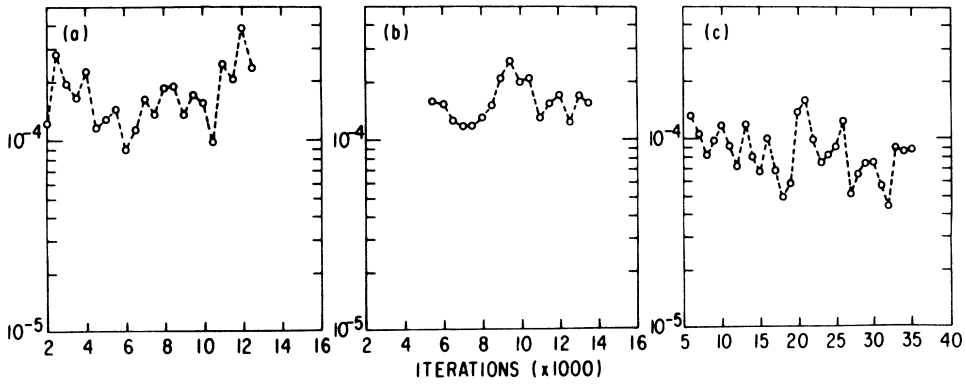

FIG. 7. Pion propagator at time slice 17, vs iteration number, for $ma=\tilde{m}a=0.05$, $n_f=3$, $\beta=5.70$, and $V=10^3\times 32$. The acceptance is 70% (a), 81% (b), and 89% (c).

on the same configuration were removed at a time. Such a jackknife would thus probe correlation intervals of 1000 (2000) iterations, which is about the same as the range of the fluctuations observed in the pion propagator. For each value of the lattice parameters, samples of 3×25 to 3×30 propagators were considered (see Table I).

The propagators were calculated for different values of the mass $\tilde{m}$, $0.01\leq\tilde{m}a\leq0.50$, in order to study the effects of the valence quarks of masses different from those of the dynamical $q\bar{q}$ pairs. Residues ranging from 10^{-8} ($\tilde{m}a=0.50$) to 10^{-6} ($\tilde{m}a=0.02$) were typically achieved with 100 to 500 conjugate-gradient iterations.[15]

The finite extent of the lattice in the temporal direction will induce important contributions from excited hadronic states, which will be reflected in nonzero amplitudes $A_{n>1}$ and $\tilde{A}_{n>1}$ in Eq. (2.10). These can be isolated or suppressed by fitting the propagators at large $|t-t_0|$ or by including such amplitudes in the fits. The problem with the former is that it reduces the number of data points in the fit; the latter, on the other hand, uses all points but involves many parameters to be fitted. These two problems do reduce the quality of the fits, but in different ways. Therefore, a comparison of the lowest mass extracted from these two approaches can give an objective estimate of the lowest mass involved in the channel under consideration.

The hadron propagators were fitted to Eq. (2.10) in the interval $t_{\min}<t<(N_t-t_{\min})$. Several values of $t_{\min}$ were tried (i.e., $t_{\min}=0,1,2,\ldots,6$) until the masses stabilized and the fit gave a reasonable χ^2. Several fits were also made by adding or removing terms corresponding to excited states. For example, in the mesonic channels represented by $S(1,x)$ propagators, fits with one state in the direct parity channel (i.e., $A_1\neq0$, $A_{n>1}=0$, $\tilde{A}_{n\geq1}=0$) were compared to fits with two states in the direct parity channel (i.e., $A_1, A_2\neq0$). A similar comparison was done for the $S_{(2,x)}$, $S_{(3,x)}$, and $S_{(4,x)}$ meson propagators, with fits involving one direct and one opposite parity channel (i.e., $A_1, \tilde{A}_1\neq0$) and those involving two direct and one opposite-parity channel ($A_1, A_2, \tilde{A}_1\neq0$). Finally, the four baryonic propagators were combined into a less noisy form,[25] and then fitted with one direct and one opposite-parity channel.

In general, we have observed that, in the case of the $S_{(3,x)}$ and $S_{(4,x)}$ mesonic propagators, the fits with excited states (i.e., $A_2\neq0$) were not very stable with respect to a variation of $t_{\min}$. The fits for the mesonic $S_{(1,x)}$ and $S_{(2,x)}$, on the other hand, achieved stability for much smaller values of $t_{\min}$ than for the fits containing no excited states (i.e., $A_2=0$). In their respective range of stability, both fits showed consistent (within error) values for the lowest hadron masses m_1 and $\tilde{m}_1$.

Most $A_1, \tilde{A}_1\neq0$ fits were seen to be stable for $t_{\min}=4,5,6$. In Tables III–V we show the resulting lowest hadron masses at $t_{\min}=4$ in the case of the $S_{(2,x)}$, $S_{(3,x)}$, and $S_{(4,x)}$ mesons. For the $S_{(1,x)}$ meson propagators, the masses come from a fit with two states in the direct parity channel at $t_{\min}=0$; for the baryon, the masses come from $A_1, \tilde{A}_1\neq0$ fits at $t_{\min}=6$.

IV. RESULTS

A. A comparison with the hybrid algorithm

It is useful to compare directly the hadronic spectroscopy obtained from different updating algorithms such as the pseudofermion, Langevin or hybrid methods, at the same values of the quark mass, gauge coupling, and lattice volume. To this end we have compared the Wilson loop (here measured every 10 sweeps) and several hadronic masses with those calculated by Gottlieb *et al.*[13,28] using the hybrid algorithm. For this calculation we have adopted their values of the parameters, i.e., $\beta=5.47$, $ma=0.05$, $n_f=2$, and a lattice size of $10^3\times24$. In our pseudofermion runs we have used acceptances 81% and 90% (the masses were calculated with acceptance 81% only) accumulating 16 000 and 12 000 iterations, respectively (including thermalization). The hybrid algorithm runs were performed with a step size of $\Delta\tau=0.04$ using 1000 trajectories.[13] The propagators were measured every two trajectories.

To carry out the comparison we have analyzed the scalar and the vector meson propagators of Ref. 13 using our own fitting package. The stability of the fits was checked upon the removal of several points at both ends of the hadron propagator. The masses quoted here have been obtained with exponentials corresponding to two direct parity channels (the scalar propagator) and to two direct, one opposite-parity channels (the vector propagator).

Figure 8 shows the results of our comparison. Within the margin of error, there is an agreement in the case of pion and ρ masses, as well as the excited state in the direct channel and the opposite-parity state of the $S_{(2,x)}$ spectrum. As hinted by the excited state in the $S_{(1,x)}$

TABLE III. Hadronic masses vs the acceptance. The propagator mass ($\tilde{m}a$) is the same as the dynamical quark mass (ma).

Hadron	ma: 0.05 Acc (%):70	0.05 81	0.05 89	0.10 70	0.10 81
π	0.561(7)	0.575(6)	0.597(6)	0.791(8)	0.772(9)
ρ	0.713(41)	0.725(21)	0.711(19)	0.923(9)	0.904(11)
ρ'	0.736(51)	0.756(25)	0.702(23)	0.971(9)	0.918(13)
$a_1(1^{++})$	0.988(60)	0.978(37)	0.899(27)	1.199(19)	1.208(9)
π'	0.562(36)	0.600(21)	0.579(50)	0.874(13)	0.838(16)
$f_0(0^{++})$	0.802(16)	0.812(17)	0.732(10)	1.032(8)	1.031(11)
$N(1/2^+)$	1.186(30)	1.249(41)	1.274(14)	1.518(33)	1.422(41)

TABLE IV. Hadronic masses vs the acceptance, for $ma \neq \tilde{m}a$. Here, $ma = 0.05$.

Hadron	$\tilde{m}a$: 0.50 Acc (%): 70	0.50 81	0.50 89	0.10 70	0.10 81	0.10 89	0.02 70	0.02 81	0.02 89
π	1.654(1)	1.654(2)	1.653(6)	0.779(3)	0.783(7)	0.794(3)	0.380(12)	0.401(9)	0.476(13)
ρ	1.817(4)	1.836(5)	1.812(2)	0.919(6)	0.925(12)	0.904(11)	0.592(11)	0.589(41)	0.664(21)
$a_1(1^{++})$	2.173(15)	2.035(22)	2.096(12)	1.194(39)	1.190(20)	1.119(15)	0.819(65)	0.841(57)	0.808(31)
$f_0(0^{++})$	1.989(24)	1.991(23)	1.989(12)	1.031(14)	1.045(27)	0.972(73)	0.628(51)	0.688(37)	0.589(25)
$N(1/2^+)$	2.867(7)	2.862(24)	2.862(7)	1.540(31)	1.513(30)	1.526(37)	1.167(140)	1.396(276)	1.418(150)

channel, the masses from the pseudofermion approach appear to be systematically higher than those of the hybrid calculation (see also Tables III and V).

The comparison of the Wilson loop is also shown in Fig. 8. The loops differ by less than 1% (91% acceptance) and 2% (81% acceptance). Here the pseudofermion algorithm has produced the smaller values (see also Tables III–V). Linearly extrapolating those two points to $\rho = 0$ would give a value 0.540 6(4)—still lower than the hybrid value. It has to be stressed however that the results of Fig. 2 at $ma = 0.05$ do not support a linear extrapolation in the present range of acceptances, and suggest instead a higher extrapolated value, presumably much closer to the hybrid value, or perhaps even higher. Let us point out that for the sake of a complete comparison between the two algorithms it would be useful to have data obtained with the hybrid algorithm for many values of the step $\Delta\tau$.

The difference between the two updating schemes can be understood from the fact that the typical step sizes ρ and $d\tau$ are of the same order of magnitude and that the hybrid algorithm includes derivatives approximated by second-order finite differences, in contrast with the pseudofermion method, which uses a first-order discretization [see Eq. (2.5)]. Most approximate algorithms tend to not include all of the necessary fermion polarization during the update, leading to more disordered gauge configurations, and hence to a lower Wilson loop and higher hadronic masses.

A similar comparison between the pseudofermion algorithm and the hybrid algorithm has been carried out by Born *et al.*[14] at $\beta = 5.20$, with a similar outcome.

B. Hadronic spectroscopy

We now turn to the hadronic spectroscopy which can be inferred from our calculation (see Tables III and IV).

TABLE V. Comparison of hadronic masses, hybrid vs pseudofermion algorithm. Here $ma = \tilde{m}a = 0.05$, $V = 10^3 \times 24$, $n_f = 2$, $\beta = 5.47$.

	Hybrid Ref. 13 published	Hybrid Ref. 13 recalculated	Pseudofermion (81% acceptance)
π	0.6099(10)	0.6116(20)	0.6083(23)
ρ	0.937(45)	0.989(30)	1.170(330)
$m_2^{\pi(d)}$		1.485(10)	1.779(11)
$m_2^{\rho(d)}$		1.60(17)	1.70(23)
$m_1^{\rho(a)}$		1.69(10)	1.75(12)

The masses for which $\tilde{m}$ is equal to m allow us to study the light-quark sector of QCD; those for which $\tilde{m}$ is different from m can, on the other hand, provide useful information about charmed (and heavier) mesons and baryons.

As discussed in Sec. III A, it may be difficult to extrapolate with respect to $\rho/(ma)^2$, due to the still large values of that ratio (see Table I). At best, extrapolating linearly or quadratically can provide a rough estimate of the errors involved. The only thing we can do in these circumstances is therefore to use the data which correspond to similar values of $\rho/(ma)^2$, i.e., use those masses computed at $ma = 0.05$ from 89% acceptance runs, and those at $ma = 0.10$ from 70% acceptance (see Fig. 2).

In studying first the meson containing the u,d quarks (i.e., $m = \tilde{m}$), we obtain the following mass ratios of proton to ρ and of pion to ρ:

$$\frac{m_p}{M_\rho} = 1.64(5), \quad ma = 0.10 , \tag{4.1}$$

$$\frac{M_p}{M_\rho} = 1.79(7), \quad ma = 0.05 , \tag{4.2}$$

and

$$\frac{M_\pi}{M_\rho} = 0.86(2), \quad ma = 0.10 , \tag{4.3}$$

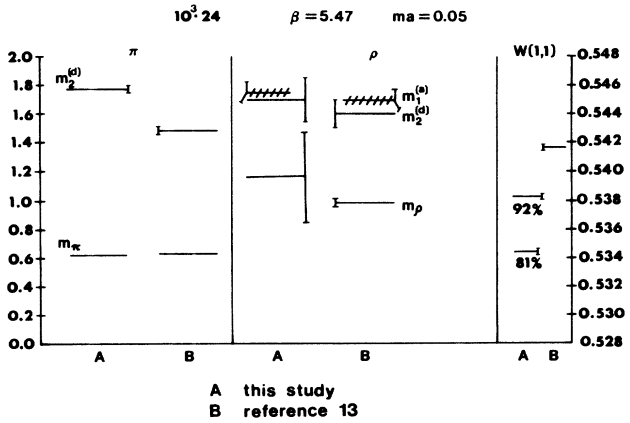

FIG. 8. Comparison of hadronic masses, hybrid vs pseudofermion, $ma = \tilde{m}a = 0.05$, $\beta = 5.47$, $n_f = 2$, and $V = 10^3 \times 24$. $m_2^{(d)}$ corresponds to the second excited state in the direct-parity channel, $m_1^{(a)}$ the first state in the opposite-parity channel.

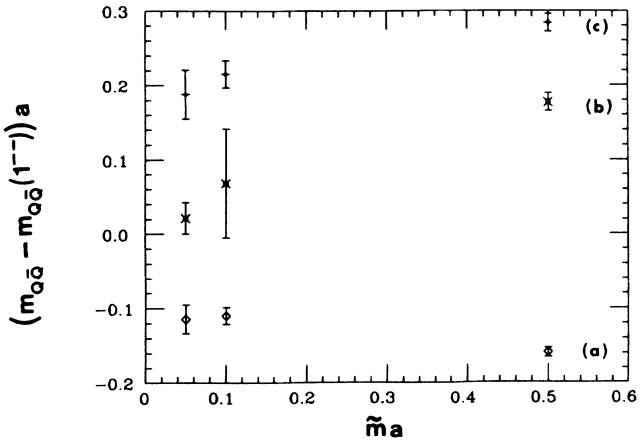

FIG. 9. Mass splittings (a) $\eta_c - J/\psi$, (b) $\eta_{c0} - J/\psi$, and (c) $\eta_{c1} - J/\psi$ vs the propagator mass $\tilde{m}a$.

$$\frac{M_\pi}{M_\rho} = 0.84(3), \quad ma = 0.05 \ . \tag{4.4}$$

It appears that the presence of the dynamical fermions of mass 0.05 and 0.10 does not help to bring M_p/M_ρ down to its experimental value of 1.2. Our values are consistent with most of those obtained from the quenched approximation.

A physical value for the lattice spacing can be extracted by extrapolating to the zero quark mass limit and by using the experimental value of the ρ mass. We obtain

$$a^{-1} = 1540(100) \text{ MeV} \ . \tag{4.5}$$

We now turn to the charm spectroscopy[29–31] which can be inferred from the $\tilde{m}a \neq ma$ data [see Table IV]. Here the 0^{+-}, 1^{--}, 0^{++}, and 1^{++} states would correspond to the η_c, J/ψ, η_{c0}, and η_{c1}, respectively. The presence of the heavy quark introduces another scale which needs to be fixed by using experimental data.[32,33] To this end, we use Eq. (4.5) and the data of our J/ψ-like meson state (the 1^{--} state) and compare that with the experimental mass of the η_c; by extrapolating linearly in the range $\tilde{m}a > 0.05$, we obtain

$$m_Q a = 0.57(7) \tag{4.6}$$

or $m_Q = 878(111)$ MeV, again using Eq. (4.5). [We get $m_Q = 970(123)$ MeV when using the 0^{+-} state and the mass of the η_c.] Our "lattice renormalized" heavy-quark mass m_Q is in the general range of values obtained from potential models:[29] $0.9 < m_Q < 1.6$ GeV. Let us stress here that m_Q is renormalization-scheme dependent and therefore varies widely from one model to another.

In Fig. 9 we show the splitting $m_{\eta_c} - m_{J/\psi}$, $m_{c_0} - m_{J/\psi}$, $m_{\eta_{c1}} - m_{J/\psi}$ in lattice units versus the propagator quark mass $\tilde{m}a$. These can be compared at m_Q [see Eq. (4.6)] with their experimental values which, in units defined by Eq. (4.5), are given by $-0.076(5)$, 0.206(13), and 0.268(17), respectively. The few data points and the large errors prevent any clear signal for behavior of the type $1/\tilde{m}$ or $1/\tilde{m}^2$ which are expected from the kinematics and the spin interactions.

V. CONCLUSION

We have described a large-scale calculation of the hadronic mass spectrum in lattice QCD. The effects of the dynamical quarks were included via the use of the pseudofermion algorithm. The systematic errors of this algorithm were monitored over a wide range of acceptances and over two values of the dynamical quark mass and of the gauge couplings.

At $\beta = 5.7$, we have seen that a 5–10% systematic error was introduced by the pseudofermion algorithm in the hadron mass calculation. In the case of the Wilson loop factors, on the other hand, variations of the acceptance rate in the range 60–90% induced changes of order 1% in $W(1,1)$ and of order 5% for $W(3,3)$, both for $ma = 0.10$ and 0.05. A more important issue was the extrapolation to 100% acceptance, or as we have suggested, to $\rho/(ma)^2 = 0.0$, which ultimately removes the updating systematic error. We have seen a linear behavior in both hadronic masses and plaquette variable in the case $ma = 0.10$; however, since $\rho/(ma)^2 > 1$, no linear extrapolation could be taken seriously. For $ma = 0.05$, on the other hand, nonlinear behavior was seen in both plaquette and hadronic mass data.

With the coupling $\beta = 5.47$, we could compare our results with those obtained with the hybrid algorithm.[13] Our Wilson loop factors were found to be smaller by about 1–2%; hadronic masses were typically higher than those of the hybrid algorithm by 2–10%, depending on the state. From our experience at $\beta = 5.7$, we expect these differences to be substantially reduced by going to higher acceptance. We understand these differences to come from the fact that, for similar step sizes ρ and $\Delta\tau$, the errors in the hybrid algorithm are smaller than those of the pseudofermion because derivatives are approximated by higher-order finite differences. It would be very interesting to compare with hybrid data obtained from simulations done for more than one value of the step $\Delta\tau$. For the moment, we believe that the issue concerning which algorithm is best cannot be settled until such data are available.

We have also verified that our simulation was done on the low-temperature (or confining) side of the QCD phase transition, for all values of the quark masses and acceptances. We have estimated the inverse lattice spacing of our simulation at $a^{-1} = 1540(100)$ MeV; the proton-to-ρ and pion-to-ρ mass ratios were found to be consistent with those of the quenched approximation. In the "charmed" sector of the spectrum, we have estimated the heavy-quark mass scale to be 878–970 MeV.

ACKNOWLEDGMENTS

We thank S. Gottlieb and D. Toussaint for sending us their hadron propagators. We are also grateful to Ph. de Forcrand, M. Fukugita, R. V. Gavai, E. Laermann, S. Sanielevici, and I. Stamatescu for numerous discussions. We would like to thank John Buchanan, Terence R. B. Donahoe, and Don Cameron of the Government of Nova Scotia and Robert M. Price of Control Data Corporation

for their continued interest, support, and encouragement and grant support; and the National Allocation Committee for the John von Neumann National Supercomputer Center for access to the two CDC CYBER 205's and the two ETA-10's at JVNC (Grants Nos. 110128, 171805, E171805, 171812, E171812, 171813, 551701-551705) where these calculations were performed. We acknowledge the support of the U.S. Department of Energy (DOE Contract No. DE-AC02-86ER40284), the Natural Sciences and Engineering Research Council of Canada (Grants Nos. NSERC A8420 and NSERC A9030), and the Canada and Nova Scotia Technology Transfer and Industrial Innovation Agreement (Grants Nos. 87TTII01 and 88TTII01).

[1]I. Montvay, Rev. Mod. Phys. **59**, 263 (1987).

[2]M. Fukugita, in *Field Theory on the Lattice,* proceedings of the International Symposium, Seillac, France, 1987, edited by A. Billoire *et al.* [Nucl. Phys. B (Proc. Suppl.) **4** (1988)].

[3]E. Marinari, in *Lattice '88,* proceedings of the International Symposium, Batavia, Illinois, 1988, edited by A. S. Kronfeld and P. B. Mackenzie [Nucl. Phys. B (Proc. Supp.) **9**, 209 (1989)].

[4]E. Marinari, G. Parisi, and C. Rebbi, Nucl. Phys. **B190**, 734 (1981), D. Weingarten, Phys. Lett. **109B**, 57 (1982).

[5]R. Kenway, in *Field Theory on the Lattice* (Ref. 2), p. 194; K. C. Bowler, C. B. Chalmers, R. D. Kenway, D. Roweth, and D. Stephenson, Nucl. Phys. **B296**, 732 (1988); D. Barkai, K. J. M. Moriarty, and C. Rebbi, Phys. Lett. **156B**, 385 (1985); P. Bacilieri *et al.*, Phys. Lett. B **214**, 115 (1988).

[6]R. Gupta, G. Guralnik, G. Kilcup, A. Patel, S. R. Sharpe, and T. Warnock, Phys. Rev. D **36**, 2813 (1987).

[7]Y. Iwasaki, in *Field Theory on the Lattice* (Ref. 2), p. 130; Y. Iwasaki and T. Yoshie, Phys. Lett. B **216**, 387 (1989); R. Sommer, Ph. de Forcrand, S. Güsken, K.-H. Mütter, A. Patel, K. Schilling, and R. Gupta, in *Field Theory on the Lattice* (Ref. 2), p. 147.

[8]M. Fukugita, Y. Oyanagi, and A. Ukawa, Phys. Rev. D **36**, 824 (1987); Phys. Lett. B **203**, 145 (1988); Y. Koike, M. Fukugita, and A. Ukawa, report, 1988 (unpublished).

[9]M. Campostrini, K. J. M. Moriarty, J. Potvin, and C. Rebbi, Phys. Lett. B **193**, 78 (1987).

[10]M. P. Grady, D. K. Sinclair, and J. B. Kogut, Phys. Lett. B **200**, 149 (1988).

[11]H. W. Hamber, A. Billoire, and E. Marinari, Phys. Lett. B **184**, 381 (1987); H. W. Hamber, *ibid.* **193**, 292 (1987).

[12]A. Patel, R. Gupta, G. W. Kilcup, and S. R. Sharpe, Phys. Lett. B **225**, 398 (1989).

[13]S. Gottlieb, W. Liu, D. Toussaint, R. L. Renken, and R. L. Sugar, Phys. Rev. D **38**, 2245 (1988).

[14]K. D. Born, E. Laermann, N. Pirch, T. F. Walsh, and P. M. Zerwas, Phys. Rev. D **40**, 1653 (1989).

[15]J. Potvin, in *Lattice Gauge Theory '86,* proceedings of the NATO Advanced Research Workshop, Upton, New York, edited by H. Satz, I. Harrity, and J. Potvin (NATO Advanced Study Institute, Series B: Physics, Vol. 159) (Plenum, New York, 1987); J. Potvin, M. Campostrini, K. J. M. Moriarty, and C. Rebbi, in *Field Theory on the Lattice* (Ref. 2), p. 140; M. Campostrini, K. J. M. Moriarty, J. Potvin, and C. Rebbi, Can. J. Phys. **67**, 792 (1989).

[16]M. Campostrini, K. J. M. Moriarty, J. Potvin, and C. Rebbi, Comput. Phys. Commun. **50**, 395 (1988).

[17]F. Fucito, M. Marinari, G. Parisi, and C. Rebbi, Nucl. Phys. **B180**, 369 (1981); H. W. Hamber, E. Marinari, G. Parisi, and C. Rebbi, Phys. Lett. **124B**, 99 (1983).

[18]Ph. de Forcrand and I. O. Stamatescu, Nucl. Phys. **B261**, 613 (1985); I. O. Stamatescu, Nucl. Phys. (Proc. Suppl.) (to be published).

[19]G. Batrouni, G. R. Katz, A. S. Kronfeld, G. P. Lepage, B. Svetitsky, and K. G. Wilson, Phys. Rev. D **32**, 2736 (1985); A. Ukawa and M. Fukugita, Phys. Rev. Lett. **55**, 1854 (1985); S. Duane, Nucl. Phys. **B257** [FS14], 652 (1985); J. B. Kogut, *ibid.* **B270** [FS16], 169 (1986).

[20]A. Kennedy, in *Field Theory on the Lattice* (Ref. 2), p. 576.

[21]A. Billoire, Ph. de Forcrand, and E. Marinari, Nucl. Phys. **B270** [FS16], 33 (1986).

[22]R. V. Gavai, A. Gocksch, and U. M. Heller, Nucl. Phys. **B283**, 381 (1987).

[23]M. Campostrini, G. Curci, and P. Rossi, Nucl. Phys. (to be published); E. Marinari, G. Parisi and C. Rebbi *ibid.* **B190** [FS3], 734 (1981).

[24]See, for example, M. Creutz, L. Jacobs, and C. Rebbi, Phys. Rep. **93**, 201 (1983).

[25]See, for example, D. Barkai, K. J. M. Moriarty, and C. Rebbi, Phys. Lett. **156B**, 385 (1985).

[26]S. Gottlieb, P. B. Mackenzie, H. B. Thacker, and D. Weingarten, Nucl. Phys. **B263**, 704 (1986).

[27]Our one-pass implementation has been described in detail in D. Barkai, K. J. M. Moriarty, and C. Rebbi, Comput. Phys. Commun. **36**, 1 (1985).

[28]S. Gottlieb, W. Liu, R. L. Renken, R. L. Sugar, and D. Toussaint, in *Lattice '88* (Ref. 3), p. 259.

[29]W. Kwong, J. L. Rosner, and C. Quigg, Annu. Rev. Nucl. Part. Sci. **37**, 325 (1987); C. Quigg and J. L. Rosner, Phys. Rep. **56**, 167 (1979).

[30]M. Campostrini, K. J. M. Moriarty, and C. Rebbi, Phys. Rev. D **36**, 3450 (1987); M. Campostrini, Phys. Lett. **147B**, 343 (1984).

[31]See the review by R. Gupta, in *Lattice Gauge Theory Using Parallel Processors,* proceedings of the CCAST Symposium, Beijing, China, 1987, edited by X. Li, Z. Qiu, and H. G. Ren (Gordon and Breach, New York, 1987).

[32]See Hamber (Ref. 11) and also in *Nonperturbative Methods in Field Theory,* proceedings of the Symposium, Irvine, California, 1987, edited by H. W. Hamber [Nucl. Phys. B (Proc. Suppl.) **1A**, 133 (1987)].

[33]R. D. Loft and T. A. DeGrand, Phys. Rev. D **39**, 2678 (1989).